Aβ Oligomers and Fibrillar Aggregates Induce Different Apoptotic Pathways in LAN5 Neuroblastoma Cell Cultures

Pasquale Picone,[†‡] Rita Carrotta,[§] Giovanna Montana,[‡] Maria Rita Nobile,[‡] Pier Luigi San Biagio,[§] and Marta Di Carlo[‡*]

[†]Dipartimento di Chimica e Tecnologie Farmaceutiche, University of Palermo, [‡]Istituto di Biomedicina ed Immunologia Molecolare CNR, and [§]Istituto di BioFisica CNR, Palermo, Italy

ABSTRACT Fibril deposit formation of amyloid β-protein (Aβ) in the brain is a hallmark of Alzheimer's disease (AD). Increasing evidence suggests that toxicity is linked to diffusible Aβ oligomers, which have been found in soluble brain extracts of AD patients, rather than to insoluble fibers. Here we report a study of the toxicity of two distinct forms of recombinant Aβ small oligomers and fibrillar aggregates to simulate the action of diffusible Aβ oligomers and amyloid plaques on neuronal cells. Different techniques, including dynamic light scattering, fluorescence, and scanning electron microscopy, have been used to characterize the two forms of Aβ. Under similar conditions and comparable incubation times in neuroblastoma LAN5 cell cultures, oligomeric species obtained from Aβ peptide are more toxic than fibrillar aggregates. Both oligomers and aggregates are able to induce neurodegeneration by apoptosis activation, as demonstrated by TUNEL assay and Hoechst staining assays. Moreover, we show that aggregates induce apoptosis by caspase 8 activation (extrinsic pathway), whereas oligomers induce apoptosis principally by caspase 9 activation (intrinsic pathway). These results are confirmed by cytochrome *c* release, almost exclusively detected in the cytosolic fraction of LAN5 cells treated with oligomers. These findings indicate an active and direct interaction between oligomers and the cellular membrane, and are consistent with internalization of the oligomeric species into the cytosol.

INTRODUCTION

Alzheimer's disease (AD) is the most common form of senile dementia and is characterized by a progressive neuronal loss causing memory deficits, cognitive impairment, disorientation, and language problems. Despite intensive research, no effective therapy for AD is currently available. The histopathological hallmarks for the disease are senile plaques and neurofibrillar tangles, which cause synaptic dysfunction with subsequent neuronal death, especially in the neurocortical regions involved in memory and motor processing (1–3). Senile plaques form in the extracellular space and consist of a proteinaceous core composed mainly of amyloid β (Aβ)-peptides. Neurofibrillar tangles are formed by neuronal intracellular deposition of the microtubule-associated Tau protein (4). The extracellular Aβ deposits found in patients with AD contain ordered aggregates called amyloid fibrils. The Aβ-peptides, which exist as distinct peptides 39–42 amino acids long, are a product of the sequential γ- and β-secretase proteolytic cleavage of the amyloid precursor protein (APP) (5). APP is a transmembrane protein of unknown function that is expressed in the heart, kidneys, lungs, spleen, intestine, and brain (6). In vitro, the more pathological Aβ-peptide form, Aβ42, has a high tendency to polymerize and make fibrils, converting its conformation to a β-rich structure (7). Small oligomers have also been found in the intracellular environment and the cerebrospinal fluid of AD patients (8). This evidence, together with the low correlation between brain cell damage and plaques formation, supports the hypothesis that ''soluble oligomers'' rather than mature amyloid fibrils are the early pathogenic agents in AD (9–14).

In vitro, Aβ42 forms fibrils that are similar to those found in AD plaques. Depending on the pH conditions, it is possible to obtain samples that contain mainly small oligomers or larger aggregates (15). The structural features of fibrillar aggregates formed at pH 3.1 at the late stage of the Aβ40 aggregation process have been described in a model obtained with a combination of different scattering techniques (16). Using a recombinant Aβ42 peptide (rAβ42) that presents biophysics and immunological properties comparable to the natural peptide (17), we recently demonstrated that, under physiological pH conditions, rAβ42 forms small oligomers, whereas at acidic pH large fibrillar aggregates are formed. Previous toxicity assays using *Paracentrotus lividus* embryos as a eukaryotic model system demonstrated a loss of embryo vitality under incubation both with oligomers and large aggregates, with a greater effect observed for the former species (17). In the study presented here, we investigated the toxicity produced by small oligomers prepared at physiological pH, and fibrillar aggregates kept in an acidic solution at $T = 37°C$ for 4 days, in a more complex mammalian cell culture, such as human neuroblastoma LAN5 cells. The possibility of using in vitro oligomers or larger aggregates formed starting with the same recombinant peptide allowed us to simulate the pathophysiological effects that occur in vivo. The molecular species obtained under different conditions and treatments were characterized by light scattering after dilution in RPMI to ascertain that they did not aggregate and/or dissolve

Submitted July 25, 2008, and accepted for publication November 19, 2008.

*Correspondence: di-carlo@ibim.cnr.it

Editor: Heinrich Roder.

0006-3495/09/5/4200/12 $2.00

doi: 10.1016/j.bpj.2008.11.056

during the experiments of cellular growth. A different effect of oligomers and fibrillar aggregates on the cellular vitality was detected, with enhanced degeneration and cell death caused by the small oligomers. Moreover, we analyzed which cellular mechanism was involved in the degenerative process by discriminating two different apoptotic pathways through the activation of two different caspases. Our results show that the preformed fibrillar aggregates activate only the extrinsic apoptotic pathway (caspase 8). Remaining on the exterior of the cell, they could macroscopically obstruct the membrane functional space. Conversely, the oligomers activate mainly the intrinsic degenerative pathway (caspase 9). This different action suggests that the oligomers can either enter into the cell by a mechanism that is not yet understood or interact with the cellular membrane. Both mechanisms could involve some membrane receptors or the well-known ability of the Aβ-peptide to form membrane pores.

MATERIALS AND METHODS

Immunoblot

Isolation and purification of rAβ42 were performed as previously described (17). rAβ42 (10 ng) dissolved in 0.01 M Tris-HCl buffer, pH 7.2, or in 0.1 M Na-citrate buffer, pH 3.1, was electrophoretically separated using 4–12% gradient gel (NuPAGE; Invitrogen, Carlsbad, CA) and transferred onto nitrocellulose filters for immunoblotting. After blocking in 3% BSA in TBST, the Western blot was incubated with anti-His HRP conjugate (1:5000; Pierce, Appleton, WI), recognizing the polyhistidine tag (6His) linked at the NH_2 terminus of the rAβ42 peptide (17). Primary antibodies were directly detected using the ECL chemiluminescence kit (Amersham Biosciences, Buckinghamshire, UK) according to the manufacturer's instructions.

Thioflavin T staining

Recombinant Aβ42 was dissolved at pH 3.1 and pH 7.2 at a concentration of 340 μM and incubated at 37°C. Aliquots were taken immediately after dissolution (time 0) and after 24, 48, 72 and 96 h of incubation and stained, adding thioflavin T (ThT) at a final concentration of 70 μM, and applied to microscope slides. The presence of large fibrillar aggregates with dimensions in the range of micrometers was visualized with the fluorescence optics of an Axio Scope 2 microscope (Zeiss, Oberkochen, Germany). The images were captured using an AxioCam digital camera interfaced with a computer.

Preparation and characterization of rAβ42 oligomers and fibrillar aggregates

The preliminary treatment with trifluoroacetic acid (TFA) has been reported elsewhere (17). To obtain small oligomers, the powder of rAβ42 was dissolved in 0.01 M Tris-HCl buffer, pH 7.2. To obtain large fibrillar aggregates, rAβ42 was dissolved in 0.1 M Na-citrate buffer, pH 3.1, with a concentration of ~300 μM and held at $T = 37$°C for 4 days. In the former case, the solution was readily characterized by dynamic light scattering (DLS) at $T = 15$°C. In the latter case, the solution at acid pH was also characterized by DLS at $T = 15$°C after 4 days incubation at $T = 37$°C. Solutions at pH 7.2 and pH 3.1 were characterized just after dissolution by Western blot to confirm a high population of oligomeric species and larger aggregates, respectively. The aggregates' growth at pH 3.1 was further monitored during the incubation at $T = 37$°C by fluorescence microscopy on aliquots of solution stained with ThT. After 4 days incubation, the sample diluted up to 3.4 μM was dried and scanning electron microscopy (SEM) was performed to determine the aggregates' morphology.

To investigate the effect of the dilution in the cellular environment, both small oligomers prepared at physiological pH and large fibrillar aggregates made at acidic pH were diluted in RPMI without phenol red to 20 μM. In situ static light scattering (SLS) and dynamic light scattering (DLS) by both solutions, held at $T = 37$°C, were monitored for 4 h to assess the effect of the dilution in RPMI and on the temporal evolution of the samples after dilution.

Sample concentration was determined by measuring the UV absorption, using $\varepsilon_{280\text{nm}} = 1390\ \text{M}^{-1}\ \text{cm}^{-1}$.

Static and dynamic light scattering

The cuvette was placed in a thermostatically controlled cell compartment of a Brookhaven Instrument BI200-SM goniometer equipped with a 100 mW solid-state laser at $\lambda = 532$ nm. Temperature was thermostatically controlled by a circulating bath with a tolerance within 0.05°C. Scattered light intensity at $\theta = 90^\circ$ ($q = \frac{4\pi}{\lambda}\sin\frac{\theta}{2} = 22.3\mu m^{-1}$), $I_{90^\circ}(t)$, and its time autocorrelation function, $g_2(t)$, were measured simultaneously by using a Brookhaven BI-9000 correlator. The Rayleigh ratio R_{90°, measured after dilution in RPMI, was used to estimate the weight-averaged molecular mass M_w of the samples prepared from the solution at pH 3.1 and pH 7.2. In fact $R_{90^\circ} = KcM_wP(90^\circ)$, where c is the protein weight concentration, $P(90^\circ)$ is the form factor, and K is a constant that depends, in addition to the experimental setup, on the refraction index of the solution n, the laser wavelength λ, and the derivative dn/dc (taken 0.18 cm^3g^{-1}) (18). Absolute scale was obtained by normalization with respect to toluene, whose Rayleigh ratio at 532 nm was taken at $28 \times 10^{-6}\ \text{cm}^{-1}$. Autocorrelation functions $g_2(t)$ were analyzed using a smoothing constrained regularization method (19) to obtain the distribution $P(D)$ of the apparent diffusion coefficients D: $g_2(t) = 1 + B|\int P(D)e^{-Dq^2t}dD|^2$, where q is the scattering vector defined as $q = \frac{4\pi n}{\lambda_0}\sin\frac{\theta}{2}$. In this equation, θ is the scattering angle and B is a factor depending on the instrumental setup (19). Assuming the Stokes Einstein relation, we can express the apparent diffusion coefficient as a function of the z-averaged hydrodynamic radius R_h: $D = \frac{kT}{6\pi\eta R_h}$, where k is the Boltzmann constant, T is the absolute temperature, and η is the solvent viscosity. Thus we obtain the distribution $P(R_h)$ of the z-averaged hydrodynamic radius.

Scanning electron microscopy

A scanning electron microscope (XL-30; Philips, Best, The Netherlands) was used to evaluate the size and morphology of the rAβ42 aggregates, formed at pH 3.1 after incubation at 37°C for 96 h. The sample (3.4 μM) was deposited on a carbon film and dried under vacuum at room temperature. Before the SEM analysis, the dried sample was gold-coated, fixed into a sample holder, and placed in the vacuum chamber of the microscope.

Cell cultures and rAβ42 treatment

LAN5 human neuroblastoma cell lines were plated onto 96-well plates at a density of 3×10^4 per well and cultured with RPMI 1640 medium (CELBIO, Milan, Italy) supplemented with 10% fetal bovine serum (FBS; GIBCO, Auckland, New Zealand) and 1% antibiotics (50 μ/mL penicillin and 50 μg/mL streptomycin) and antimycotics (Sigma). The cells were maintained in humidified 5% CO_2 atmosphere at 37°C and treated with increasing amounts (3.75, 7.5 15, and 30 μM) of recombinant Aβ42 (rAβ42) in oligomer and aggregate forms (15). For the time-dependence experiment, the 15 μM concentration was used. Depending on the experiment, the peptides (oligomers/aggregates) were incubated at 37°C for 4 or 5 h, or for 5–24 h. The treated cultured cells and the controls were morphologically analyzed by microscopy inspection or used for specific assays. As controls we used untreated cells or cultured cells with buffer (pH 3.1, pH 7.2) in the concentration and volume utilized to dissolve rAβ42.

Immunohistochemistry

LAN5 cells were cultured on slides without or with 15 μM of rAβ42 oligomers for 24 h. After washing in PBS (137 mM NaCl, 2.7 mM KCl, 8 mM

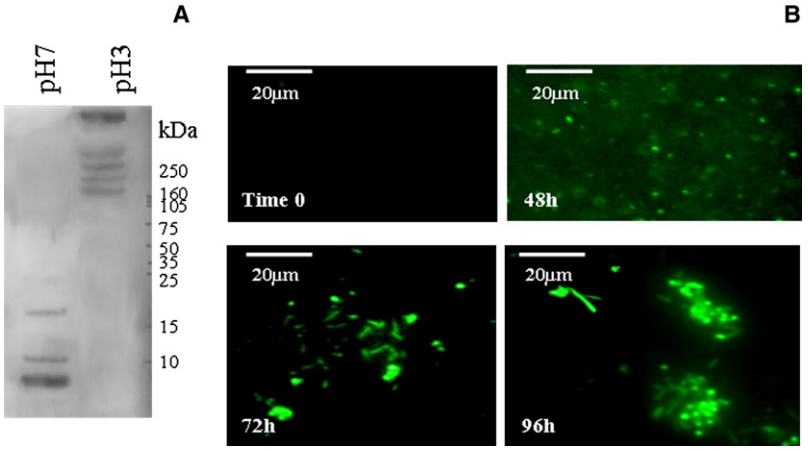

FIGURE 1 Neutral or acid rAβ42 solutions containing different structural species. (*A*) Western blot of rAβ42 immediately after dissolution at pH 7.2 (pH 7), and pH 3.1 (pH 3) incubated with anti-His. On the right, molecular weight standards are indicated. (*B*) Kinetics of fibrillar aggregates formation of rAβ42 dissolved at pH 3.1. Staining with ThT at different times of incubation at $T = 37°C$. Fluorescence images of representative areas of the observation field, immediately after dissolution (time 0) and after 48 (48 h), 72 (72 h) and 96 h (96 h) of incubation at $T = 37°C$. Bar: 20 μm.

Na_2PO_4, pH 7.4), the cells were fixed in freshly prepared 4% paraformaldehyde in PBS for 30 min and kept at 4°C. After three washes in PBS, the slides were incubated for 1 h with 5% bovine serum albumin/PBS. Then the cultures were incubated with human anti-Aβ (1:200; Santa Cruz Biotechnology, Santa Cruz, CA) or anti-His (Penta.His Alexa fluor conjugate, 1:100; QIAGEN, Hiden, Germany) antibodies at 4°C overnight. After three washes in TBS (PBS, 2% Triton X-100) the samples treated with anti-Aβ were incubated with anti-mouse Cy3-conjugate secondary antibody (1:300), whereas the samples treated with anti-His were directly detected. Fluorescent or light field images were observed with an Axio Scope 2 microscope (Zeiss) and captured with an AxioCam digital camera (Zeiss) interfaced with a computer.

Cytotoxic assay

Cell viability was measured by MTS (3-(4,5-dimethylthiazol-2-yl)-5-(3-carboxymethoxyphenyl)-2-(4-sulfopheyl)2H-tetrazolium; Promega, Madison, WI) assay according to the manufacturer's instructions. After treatment of the cells, 20 μL of the MTS solution were added to each well and the incubation was continued for 4 h at 37°C, 5% CO_2. The absorbance was read at 490 nm on a microplate reader (Wallac Victor 2 1420 multilabel counter; PerkinElmer, Waltham, MA). The absorbance of a blank RPMI sample was subtracted from all the absorption measurements corresponding to the different samples. The caspase inhibitor assay was performed with Z-VAD-FMK (50 μM; Promega).

Apoptosis assays

A terminal deoxynucleotidyl transferase dUTP nick end labeling (TUNEL) assay (Promega) was performed according to the manufacturer's instructions. Briefly, cells in oligomer or aggregate form were treated with 20 μM rAβ42 for 5 h and then fixed with 4% paraformaldehyde in PBS for 30 min. They were then washed with PBS permeabilized with 0.2% Triton X-100 in PBS for 5 min, rinsed with PBS, and incubated with a TUNEL reaction mixture (enzyme and nucleotides) in a humidified atmosphere at 37°C for 1 h. Staining was obtained by using a peroxidase substrate, hydrogen peroxide, and the stable chromogen diaminobenzidine (DAB). After these incubations, the samples were rinsed three times with PBS and analyzed under a Zeiss Axio Scope microscope. For nuclear staining, the fixed cells were incubated in Hoechst 33258 (5 μg/mL) for 20 min. Nuclear morphology was analyzed by microscopic inspection using a Leica DHL fluorescent microscope at excitation/emission wavelengths of 350/450 nm.

Caspase assays

Caspase-8, 9, 3 activities in cells were measured with the use of commercially available luminescent assays (caspase-Glo™8, caspase-Glo™ 9, and caspase-Glo™ 3/7 assay systems; Promega). LAN5 cells were treated with 20 μM oligomers or aggregates or untreated for 4 h. Caspase reagent specific for each kit was added directly to the cells in white 96-well plates, and after mixing were incubated for 15–30 min. Luminescence was recorded with a Wallac Victor 2 1420 multilabel counter (PerkinElmer) apparatus. The caspase activator assay was performed with 50 μM vinblastine (Sigma, St. Louis, MO), and the caspase inhibitor assay was carried out with 50 μM Z-VAD-FMK (Promega). The luminescence of a blank RPMI sample was subtracted from all the luminescence measurements corresponding to the different samples.

Cytochrome *c* release assay

LAN5 cells treated separately with oligomers or fibrillar aggregates were harvested. Cytosol and mitochondria fractions were prepared with the use of a mitochondria isolation kit (Pierce) according to the manufacturer's instructions. Lysates of both the fractions and controls were separated by 4–20% sodium dodecyl sulfate polyacrylamide gel electrophoresis (SDS-PAGE; (Cambrex, Rutherford, NJ) and the Western blot was incubated with 1:1000 diluted anti-cytochrome *c* (Cell Signaling Technology, Beverly, MA).

Statistical analysis

All experiments were repeated three times. Each experiment was performed in triplicate. Since the values of the pH 3 and pH 7 control buffers were very similar to those of the untreated cells, to facilitate the analysis we used the untreated cells to normalize the values of treated cells. The results are presented as mean $\pm$ standard deviation (SD).

RESULTS

Different pH values mediate rAβ42 aggregation differently

To obtain direct evidence that solutions of rAβ42 at two different pH values (7.2 and 3.1) contain different structural species (small oligomers or larger aggregates, respectively), an aliquot of the samples, immediately after dissolution in the different conditions, was loaded on a SDS PAGE. After running, the gel was transferred to nitrocellulose and the filter was incubated with anti-His. As shown in Fig. 1 *A*, we were able to determine by the molecular weight of the detected bands that monomer or small oligomers were present in the sample dissolved at pH 7.2, whereas larger aggregates

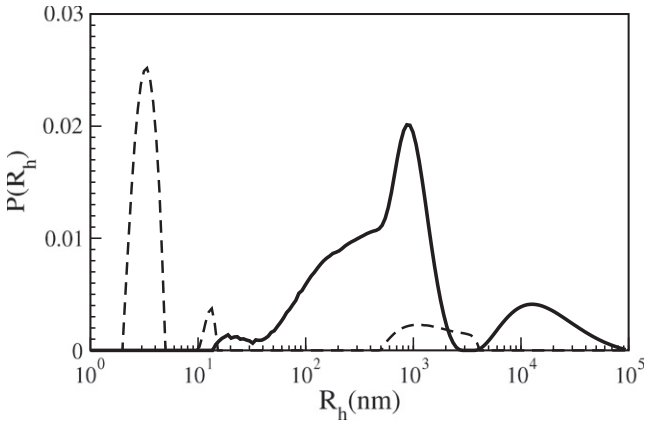

FIGURE 2 Distribution functions of the z-averaged hydrodynamic radii $P(R_h)$ obtained from the analysis of the $g_2(t)$ measured for the solution of rAβ42 at pH 7.2 (*broken line*) and pH 3.1 (*continuous line*) at $T = 15°C$. To obtain large fibrillar aggregates, the solution at pH 3.1 was incubated at $T = 37°C$ for 4 days as described in the text.

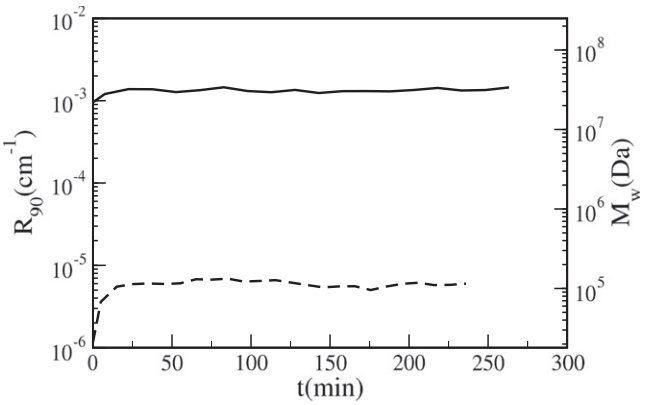

FIGURE 3 Time evolution of both the Rayleigh ratio at 90° (left y axis) and the weight-averaged molecular mass (right y axis), during incubation at $T = 37°C$. Oligomers prepared at pH 7.2 (*broken line*) and aggregates prepared at pH 3.1 (*continuous line*), immediately after dilution to 20 μM in RPMI.

starting at a molecular mass higher than 150 kDa (about 30-mer) were detected for rAβ42 immediately after dissolution at pH 3.1. Furthermore, rAβ42 neutral and acid solutions were incubated for different times at 37°C and their kinetics of aggregation was monitored after staining with ThT. No visible structures were detectable (data not shown) after staining of rAβ42 neutral solutions even after 4 days of incubation, consistent with previously reported results (17). In contrast, by monitoring rAβ42 acid solutions at different times, larger and larger structures appeared until the formation of large aggregates of dimensions up to 20 μm (Fig. 1 *B*).

Characterization of rAβ42 oligomers and fibrillar aggregates before incubation in cells

For all of the biological assays reported in this work, we used two different forms of rAβ421), oligomers of rAβ42 prepared by dissolving the peptide at physiological pH; and 2), large fibrillar aggregates obtained by incubation in an acidic solution of rAβ42 for 4 days at 37°C to simulate the two different conditions of having either small oligomers or amyloid plaques in the extracellular space. To monitor the toxic effects on LAN5 cellular growth, the two different solutions of rAβ42 were diluted in the physiological cellular medium. With the aim to control which forms of rAβ42 were present under the two different pH conditions, DLS was measured at 15°C to obtain the distribution of rAβ42 species (Fig. 2) from analysis of the intensity autocorrelation functions. As expected from previous studies (17), the dominant species at physiological pH are oligomers of dimensions $<$10 nm, whereas larger aggregates with larger dimensions (up to micrometers) are dominant in the acidic solutions (Fig. 2) (hereafter we shall indicate as oligomers a mixture of monomers and small oligomers slightly contaminated by a tiny amount of aggregates, and as aggregates a mixture of larger aggregates, from tens of nanometers to tens of micrometers). The two solutions were then diluted in RPMI (without phenol red to avoid absorption phenomena in the scattering experiments), a medium that mimics the environment of cellular growth. SLS and DLS were simultaneously measured for 4 h. The weight-averaged molecular mass after dilution was estimated from the Rayleigh ratio for both samples (Fig. 3), resulting in 25 KDa (consistent with a pentamer) for the solution made at pH 7.2, and 23 MDa for the one obtained by diluting the sample previously aggregated at acid pH. In the latter case the form factor was calculated using a rod-like model and assuming an average particle dimension of ~100 nm, $P(q = 22.3\mu m^{-1}, R = 100\ nm) \approx 0.8$ (18,19). Although this is a rough estimate, it confirms the dominant presence of large aggregates of rAβ42 starting from the sample at low pH and of oligomers diluting the solution at neutral pH. Whereas the first appears stable, a mild time dependence of the oligomer dimensions is noticed in the second, suggesting that the different milieu promotes a slightly different species distribution. After dilution the peptide concentration drops to 20 μM, with a subsequent decrease of the SLS intensity. Therefore, since the scattered intensity did not show relevant changes (Fig. 3), we chose to analyze for both samples an intensity autocorrelation function averaged for 3.5 h after 30 min from dilution, to give more reliability to the size distributions obtained after dilution. The intensity distribution of the hydrodynamic radii corresponding to the solution of fibrillar aggregates diluted in RPMI shows three distinct populations (Fig. 4 *A*): large oligomers of tens of nanometers, aggregates of hundreds of nanometers, and larger species of dimensions up to tens of micrometers. The average hydrodynamic radius as calculated from the average diffusion coefficient of the distribution ranges from 253 nm before dilution to 234 nm after dilution, pointing to a slight decrease in dimensions due to dilution. The distribution of

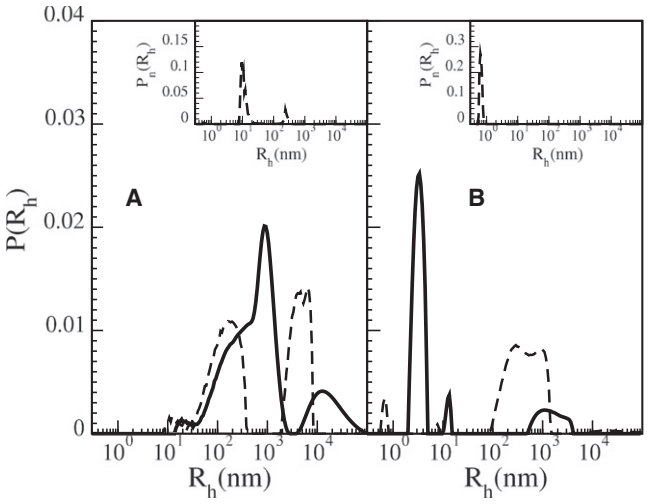

FIGURE 4 Distribution functions of the z-averaged hydrodynamic radii $P(R_h)$, corresponding to the solution of rAβ42 at pH 3.1 (*A*) before (*continuous line*) and after (*broken line*) dilution in RPMI, and at pH 7.2 (*B*) before (*continuous line*) and after (*broken line*) dilution in RPMI. For both solutions diluted in RPMI, to improve the signal/noise ratio, the analysis was performed on the intensity autocorrelation functions obtained by averaging data from 30 min to 4 h. In the insets the number distribution of the hydrodynamic radii, $P_n(R_h)$, is reported for the two solutions prepared at pH 3.1 (*A*) and pH 7.2 (*B*) after dilution in RPMI.

the hydrodynamic radii corresponding to the solution of oligomers after dilution (Fig. 4 *B*) indicates species with dimensions on the order of nanometers and the presence of a small amount of aggregates with diameters ranging from hundreds of nanometers to a few micrometers. The average hydrodynamic radius of the distribution increases from 4 nm to 15 nm with dilution. This effect could account for the marginal intensity increase observed in the first half hour (Fig. 3). After dilution (Fig. 4 *B*), although the contribution from the monomer-oligomers species accounts for only 5% of the total scattered intensity (as can be estimated by the area underneath the corresponding band), this has to be considered as the dominant species in terms of weight concentration and, even more, of number concentration (see *inset* of Fig. 4 *B*). In fact, by assuming a dependence $\frac{M_w^2}{M_w^1} = \left[\frac{R_h^2}{R_h^1}\right]^2$ (15) and an intensity contribution of $A_1 = 5\%$ and $A_2 = 95\%$ arising from species of dimensions of 1 and 100 nm, respectively, we estimated that the ratio of the number concentrations $\frac{n_2}{n_1} = \left[\frac{M_w^1}{M_w^2}\right]^2 \frac{P_1 A_2}{P_2 A_1} \cong 2.5\ 10^{-7}$, considering $P_1(q = 22.3\mu m^{-1}) = 1$ and for the larger species the form factor $P_2(q = 22.3\ \mu m^{-1}) \approx 0.8$, calculated using a rod-like model (18,19). We can therefore conclude, as shown in the number distributions reported in the insets of Fig. 4, that after dilution in RPMI the species in solution are a heterogeneous mixture of large oligomers and aggregates of hundreds of nanometers (Fig. 4 *A*, inset) in the sample prepared at pH 3.1, and mainly monomers and small oligomers (Fig. 4 *B*, inset) in the samples prepared at pH 7.2.

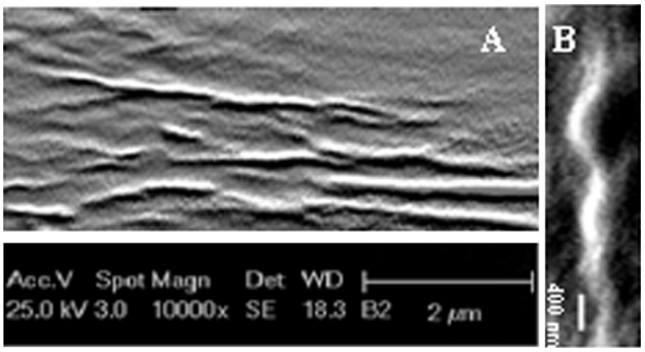

FIGURE 5 SEM images of rAβ42 aggregates formed at pH 3.1 after 4 days' incubation. (*A*) A representative overview of aggregates. (*B*) A zoom of a single aggregate, captured in a different observation field.

This analysis, together with the estimate of the weight-averaged molecular mass and the average hydrodynamic radius after dilution, strongly indicates that the sample prepared at physiologic pH contains small oligomers and a quite small amount of aggregates of dimensions in the range 100 nm–1μm. Moreover, the sample prepared at acid pH appears quite heterogeneous, with the smallest species being at least 10 times larger than the small oligomers, which are mainly present in the former solution. Furthermore, larger species (hundreds of nanometers) are significantly present in the latter solution. Concerning the largest aggregates (larger than micrometers) detected in this sample, the relative amount can be underestimated by the experimental approach used here.

Visualization of the aggregates by SEM

To examine the size and shape of the aggregates formed in acid condition, SEM was performed on the sample incubated for 4 days at $T = 37°C$ (two representative areas of the observation field are shown in Fig. 5, *A* and *B*). The SEM analysis revealed aggregates with an elongated morphology and in some cases a thread-like motif, with a helical twist typical of amyloid fibrillar superstructures (see Fig. 5 *B*). The aggregates ranged in length from hundreds of nanometers to a few micrometers, according to both the light scattering and the fluorescence microscopy results, in agreement with the model reported for the Aβ40 aggregates formed at the late stage of thermal aggregation (16).

In summary, for all of the biological assays we used two extreme conditions: 1), the rAβ42 neutral solution soon after dissolution, containing mainly small oligomers; and 2), the rAβ42 acid solution after 4 days of incubation, containing large fibrillar aggregates to simulate separately the two conditions of having in the extracellular space small oligomers or amyloid plaques that interfere with the cellular membrane in different ways.

rAβ42 binds specific cell surface sites

We then ascertained whether the recombinant peptide is able to bind to one or more specific cellular surface sites that

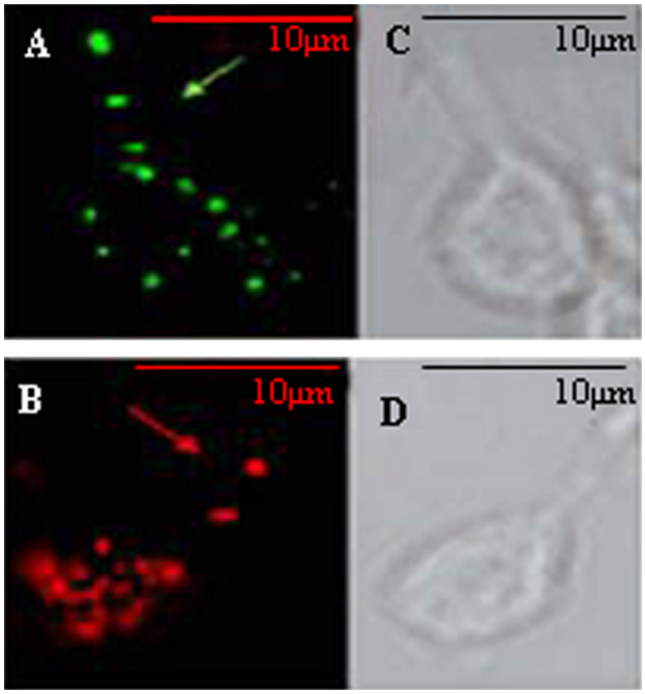

FIGURE 6 Recombinant Aβ42 binds to the neuron cell surface and shows the same punctuate staining of APP. Immunohistochemistry of LAN5 neuroblastoma cells without or with treatment of rAβ42 and incubation with anti-His (*A*) or with anti-β-amyloid (*B*), respectively. (*C* and *D*) bright field of images in *A* and *B*. Bar: 10 μm.

might potentially activate the toxic downstream pathway. LAN5 neuroblastoma cells were incubated with a solution containing rAβ42 fibrillar aggregates, and after cell fixation the rAβ42 species were localized using anti-His fluorescent antibodies (Fig. 6 *A*). Moresover, to localize APP antigen on the utilized cell line, LAN5 cells were incubated with human anti-Aβ antibodies (Fig. 6 *C*). By immunohistochemistry, a punctuate staining was detected both on the surface of the cellular body and on the neurites of treated LAN5 cells, suggesting that rAβ42 probably binds to some membrane protein or lipids, and that the employed cultures are a valid model system to simulate in vivo pathological conditions (Fig. 6, *A* and *B*). Comparable staining was detected for LAN5 cells incubated with anti-Aβ antibodies (Fig. 6, *C* and *D*).

Toxic effect of rAβ42 on human neuroblastoma LAN5 cells

We previously demonstrated in *P. lividus* embryos (17) that oligomers are more toxic than larger aggregates. To analyze whether this difference is maintained in mammalian cells, we used human neuroblastoma LAN5 cells for viability assays. In each experiment the different species in solution (oligomers or fibrillar aggregates) were monitored by light scattering. LAN5 cells were incubated with different concentrations of either aggregates at pH 3.1 (Fig. 7 *B*) or oligomers at pH 7.2 (Fig. 7 *D*). After 5 h the morphological effects with

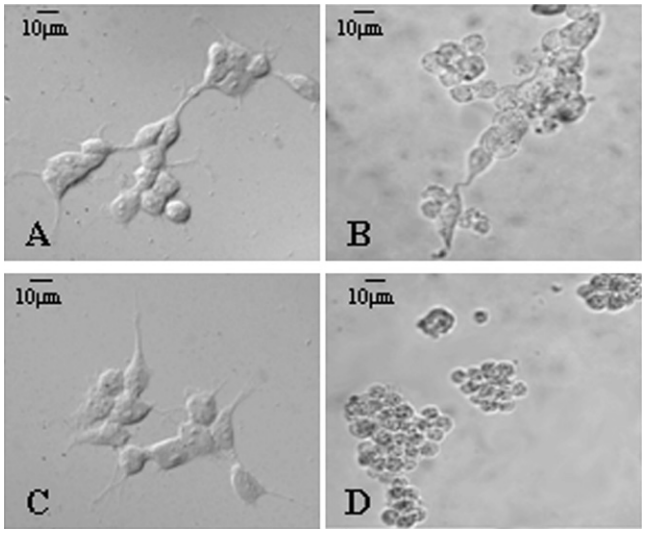

FIGURE 7 rAβ42 oligomers and fibrillar aggregates produce morphological changes in LAN5 neuroblastoma cells. Differential interference contrast image of LAN5 cells (*A*) treated with pH 3.1 buffer, (*B*) incubated with 30 μM rAβ42 aggregates, (*C*) treated with pH 7 buffer, and (*D*) incubated with 30 μM rAβ42 oligomers. The incubation lasted 5 h in each case. Bar: 10 μm.

respect to the corresponding controls (Fig. 7, *A* and *C*) were observed. Neurons at various stages of degeneration were observed (representative images are shown in Fig. 7). Morphological changes resulted in a reduction of the cellular body, neurites, and neuronal cell number.

rAβ42 oligomers and fibrillar aggregates have a different concentration and time dependence

The viability of LAN5 cells was evaluated by means of the MTS assay, using increasing amounts of either oligomers or aggregates. This assay gave results consistent with the observed morphological changes: after 5 h of treatment with aggregates or oligomers, we obtained a vitality decrease for increasing amounts of peptide. At the same concentrations, a major reduction for the oligomers treatment was always detected (IC_{50}, 11 μM for oligomers and 17 μM for aggregates) (Fig. 8 *A*). Furthermore, when we used the 15 μM peptide concentration of either oligomers or aggregates, and incubated the LAN5 cells for 5 and 24 h (Fig. 8 *B*), the MTS assays revealed a time-dependent effect and a higher toxicity for the oligomers.

rAβ42 oligomers and fibrillar aggregates induce apoptosis

Cells undergoing apoptosis are known to display morphological characteristics, including cytoplasm shrinkage, plasma membrane blebbing, chromatin condensation, and nuclear fragmentation (20). When we treated the cells with rAβ42 oligomers and aggregates, we detected morphological features in the surviving cells that were similar to the hallmarks described for apoptosis (Fig. 9). Furthermore, a drastic

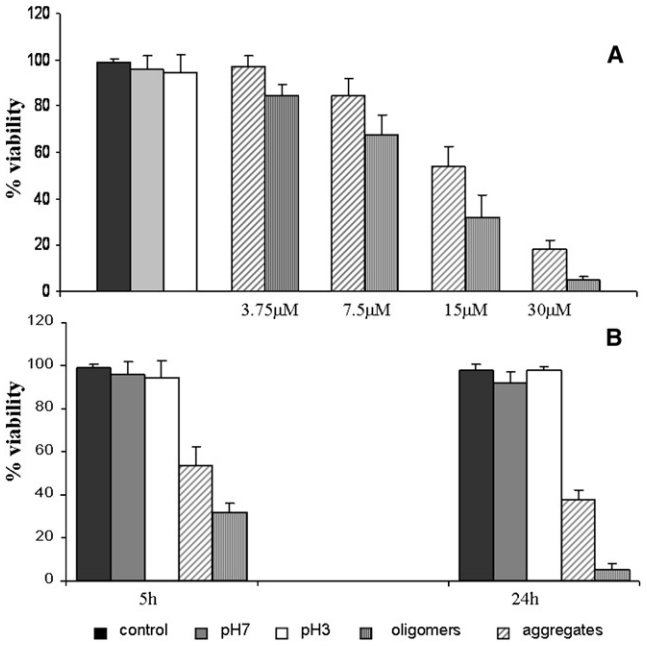

FIGURE 8 Dose and time dependence toxicity of aggregates and oligomers. Neuroblastoma LAN5 cells were incubated with oligomers and fibrillar aggregates separately at different doses and times and submitted, together with untreated cells or pH 3.1 or pH 7.2 buffer-treated cells as control, to viability MTS assays. (*A*) Percentage of viability after 5 h incubation with 3.75 μM, 7.5 μM, 15 μM, or 30 μM of aggregates and oligomers, compared with control. (*B*) Percentage of viability after incubation for 5 and 24 h with 15 μM of aggregates and oligomers, compared with control. The blank control value was subtracted from each. The data are the mean $\pm$ SD of three separate experiments, normalized with respect to control.

morphological change was observed for the surviving LAN5 cells treated with oligomers, in which granules similar to apoptotic bodies were observable. To better investigate this effect, LAN5 cells were submitted to the TUNEL assay after treatment with oligomers and aggregates for 5 h. An intense nuclear staining is visible in the cells treated with rAβ42 in both forms (Fig. 9, *B* and *C*), whereas no staining is detectable in untreated cells (Fig. 9 *A*). This result was confirmed by Hoechst 33258 staining of the nuclei. Intensive blue staining revealed the presence of DNA nicks (Fig. 9, *E* and *F*), indicating that the observed pattern of rAβ42 degeneration is consistent with an apoptotic pathway.

rAβ42 oligomers and fibrillar aggregates activate two different apoptotic pathways

Proteolytic enzymes of the caspase family play a central role in initiating and sustaining the events that result in apoptotic cell death. In some forms of apoptosis, the extrinsic apoptotic pathway is initiated by activation of caspase 8 after death receptor ligation; in others, activation of the intrinsic apoptotic pathway is initiated by signaling molecules recruited by mitochondria that produce release of cytochrome *c* from the mitochondrial matrix to cytoplasm and activation of the caspase 9 (20). Both of these pathways are able to activate the executrix caspase 3 that is involved in the death process. To identify which pathway is involved in rAβ42-induced apoptosis and to ascertain whether the difference in toxicity between oligomers and fibrillar aggregates could be due to activation of different apoptotic pathways, we performed caspase 8 and caspase 9 luminometric assays. LAN5 cells treated with oligomers and aggregates were subjected to both caspase 8 and 9 assays. A caspase activator was employed as control. Cells treated with aggregates showed a high activation of caspase 8 (Fig. 10 *A*) and a negligible activation of caspase 9 with respect to the control (Fig. 10 *B*), whereas cells treated with oligomers showed some activation of caspase 8 (Fig. 10 *A*) and a major activation of caspase 9 (Fig. 10 *B*). LAN5 cells treated as described above were employed for the caspase 3 assay and, as expected, a significant increase of the caspase 3 activity was detected (Fig. 10 *C*). Additionally, the caspase activation, when it occurred, was inhibited by the treatment of caspase inhibitor Z-VAD-FMK (Fig. 10, *A–C*).

rAβ42 toxic effect is recovered by caspase inhibitor

To ascertain whether neurotoxicity is due to induction of apoptosis, we examined the effect of a caspase inhibitor on LAN5 cells treated with oligomers and aggregates. Oligomers or aggregates were added together with the caspase inhibitor Z-VAD-FMK to LAN5 cultures. The toxicity was determined by means of the MTS assay 24 h after incubation. Oligomer or aggregate toxicity was reduced by ~50% with respect to the treated cultures, indicating that the drug developed a protective effect, and confirming that the neurodegeneration is due to caspase activation (Fig. 11).

Oligomers induce release of cytochrome *c* into the cytosol

It is known that activation of the intrinsic apoptotic pathway results in loss of mitochondrial membrane integrity and release of cytochrome *c* in the cytosol. To confirm that oligomers activate the apoptotic mitochondrial pathway, cytosolic and mitochondrial extracts from the control and LAN5 cells treated with oligomers and aggregates were separated and analyzed by Western blot. In control untreated cells, cytochrome *c* and actin were exclusively present in the mitochondrial or cytosolic fractions, respectively. In oligomer-treated cells, a decrease of the mitochondrial pool of cytochrome *c* was detected, whereas a significant amount of cytochrome *c* was present in the cytosol (Fig. 12). This is consistent with caspase 9 activation by the oligomers. Furthermore, in the aggregate-treated cells, the major part of cytochrome *c* is present in the mitochondrial fraction and a light band is present in the cytosol, probably due to the presence of a tiny amount of oligomers in the aggregates solution.

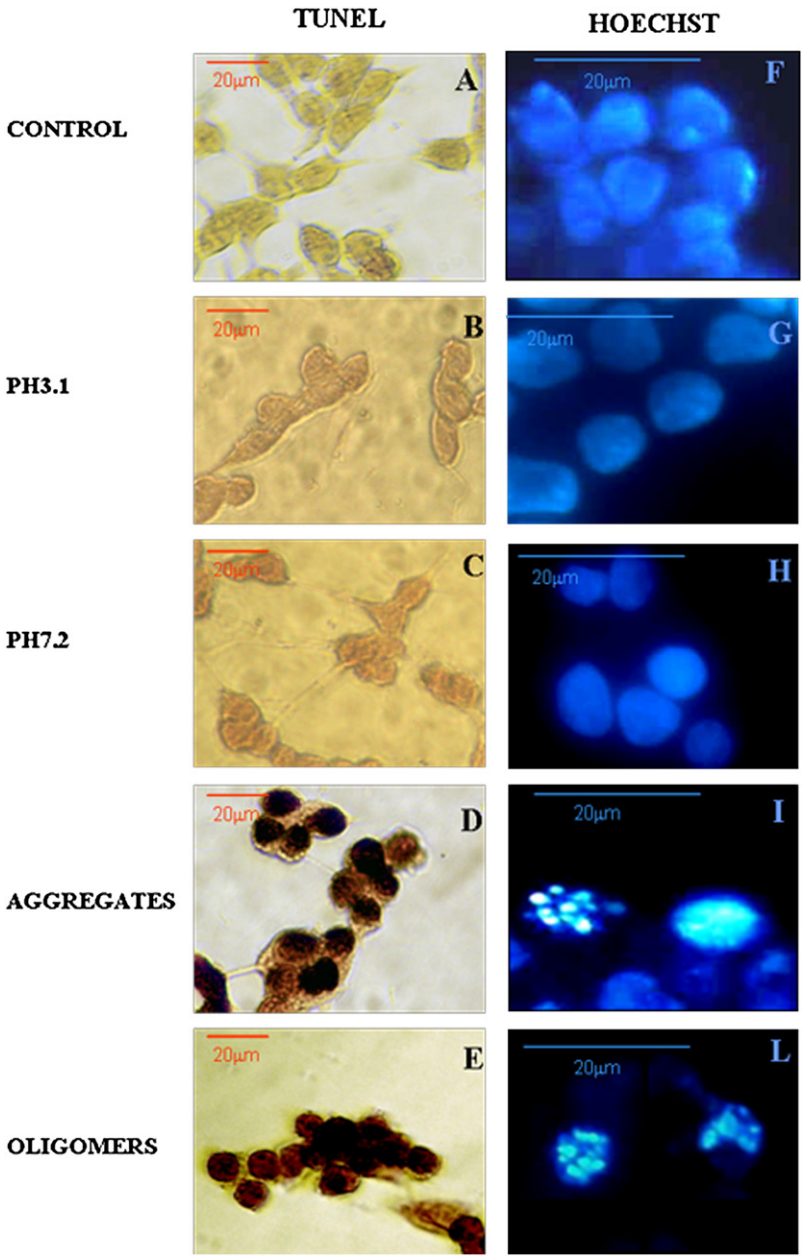

FIGURE 9 Oligomers and aggregates activate apoptosis. LAN5 untreated cells as control (*A* and *F*) or pH 3.1 (*B* and *G*) or pH 7.2 (*C* and *H*) buffers treated or treated with fibrillar aggregates (*D* and *I*) or oligomers (*E* and *L*), were fixed and submitted to TUNEL assay (*A–E*). Fragmentation of nuclei was evidenced by Hoechst 33258 staining (*F–I* and *L*). Bar: 20 μm.

DISCUSSION

This study indicates that exposure of cultured neuroblastoma LAN5 cells to both oligomers and fibrillar aggregates of rAβ42 induces degeneration and cell death via an apoptotic pathway. We provide evidence that the two species induce degeneration through two different apoptotic pathways.

The use of well-characterized oligomers or aggregates formed starting from a recombinant peptide in vitro permitted us to simulate the pathophysiological effects that occur in vivo. The experimental approach of using a recombinant Aβ-peptide, with or without amino acids mutation, was employed to correlate structure and biological activity (21). We determined the most abundant molecular species present in solution under different conditions and ascertained that they did not aggregate and/or dissolve under dilution in RPMI medium during the experiments of cellular growth. Moreover, by using immunological and microscopy techniques we were able to ascertain that for the biological assay, oligomers and large fibrillar aggregates were separately utilized. As described above, the so-called oligomers sample is actually a solution rich in small oligomers, whereas the so-called fibrillar aggregates sample is a heterogeneous solution containing aggregates with dimensions ranging from tens of nanometers to micrometers. Furthermore, we used LAN5 neuroblastoma cell lines that, as shown by immunohistochemistry, express APP antigen on their cell surface and are able to bind rAβ42.

The first relevant difference detected between oligomers and fibrillar aggregates was that oligomers produce an

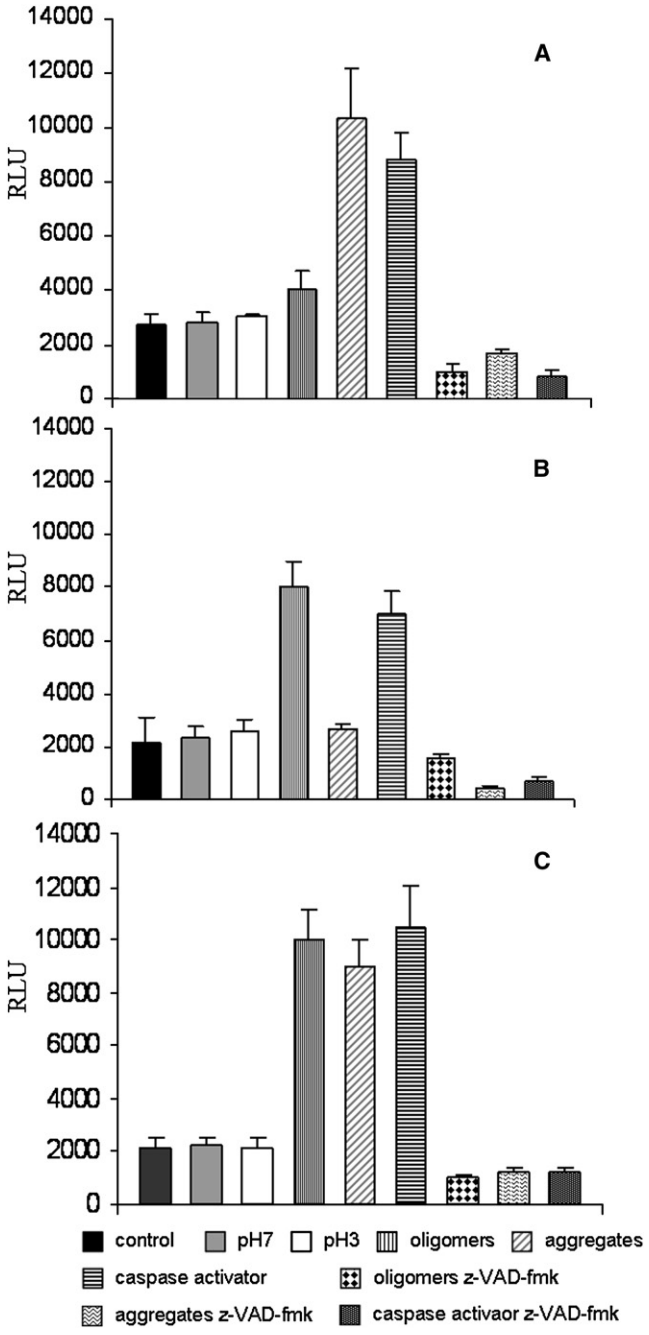

FIGURE 10 Oligomers and fibrillar aggregates activate different pathways of apoptosis. LAN5 cells were treated with aggregates, oligomers, or a caspase activator, without and with Z-VAD-FMK and submitted to caspase 8 (*A*), caspase 9 (*B*), or caspase 3 (*C*) luminescent assays. Inhibition of caspase 8 (*A*), 9 (*B*), or 3 (*C*) activation was observed after incubation of LAN5 cells with oligomers or aggregates or caspase activator plus z-VAD-fmk. Untreated cells or pH 3.1 or pH 7.2 buffer-treated cells were used as controls. On the left the relative light units are indicated. The blank control values were subtracted from each. The data are the mean ± SD of three separate experiments, normalized with respect to the control.

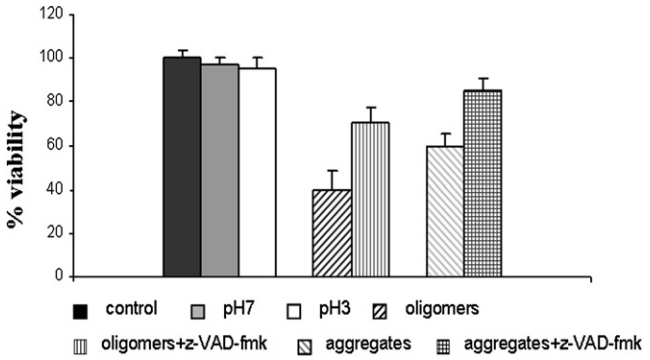

FIGURE 11 Toxicity produced by oligomers and fibrillar aggregates is reduced by the caspase inhibitor. LAN5 cells cultured in the presence of oligomers alone or with z-VAD-fmk, and with aggregates alone or with z-VAD-fmk and submitted to viability MTS assay. Untreated cells or pH 3.1 or pH 7.2 buffer-treated cells were used as controls. The corresponding blank control value was subtracted from each. The data are the mean ± SD of three separate experiments, normalized with respect to the control.

enhanced degeneration as well as cell death with respect to aggregates. This could be related to the possibility that diffusible oligomers can pass through the membrane and enter into the intracellular space. Biophysical and modeling studies have demonstrated the ability of Aβ to interact with a lipid bilayer because of its obliquity and hydrophobicity (22,23). Moreover, some evidence indicates that extracellular Aβ contributes to the intracellular pool of Aβ, and this internalization occurs via an endocytic pathway involving caveolae/lipid rafts (24).

Neuronal cultures exposed to rAβ42 exhibited DNA fragmentation and maintained cellular membrane integrity until the cells died. By using different caspase assays, we detected that the oligomers and fibrillar aggregates induced degeneration through two different apoptotic pathways. Aggregates are able to activate caspase 8 almost exclusively, whereas oligomers activate both caspase 8 and caspase 9 (although mainly caspase 9). This effect can be reversed by a caspase inhibitor that is also able to rescue a significant portion of cell death. The absence of caspase 9 activation by the aggregates suggests that these species are unable to activate an internal degenerative pathway. The evidence of cytochrome *c* release into the cytosol when cells were exposed to the oligomers agrees with caspase 9 activation, and both results suggest that oligomers can enter into the intraneuronal space.

We speculate that aggregates could mimic the extracellular plaques that perturb the cell membrane and directly or indirectly activate a death receptor, inducing an apoptotic extrinsic pathway through caspase 8 activation. Oligomers could mimic the diffusible oligomers that cross the neuron membrane and enter into the intracellular environment, where they could promote cellular mechanisms leading to activation of the apoptotic intrinsic pathway upon caspase 9-mediated signaling (Fig. 13). Furthermore, oligomers are able to activate, albeit to a minor extent, caspase 8, and this could be due to the little fraction of larger aggregates detected by light scattering in the sample at pH 7. However, we cannot exclude the possibility that small oligomer species themselves could attach to neuron surface-specific binding

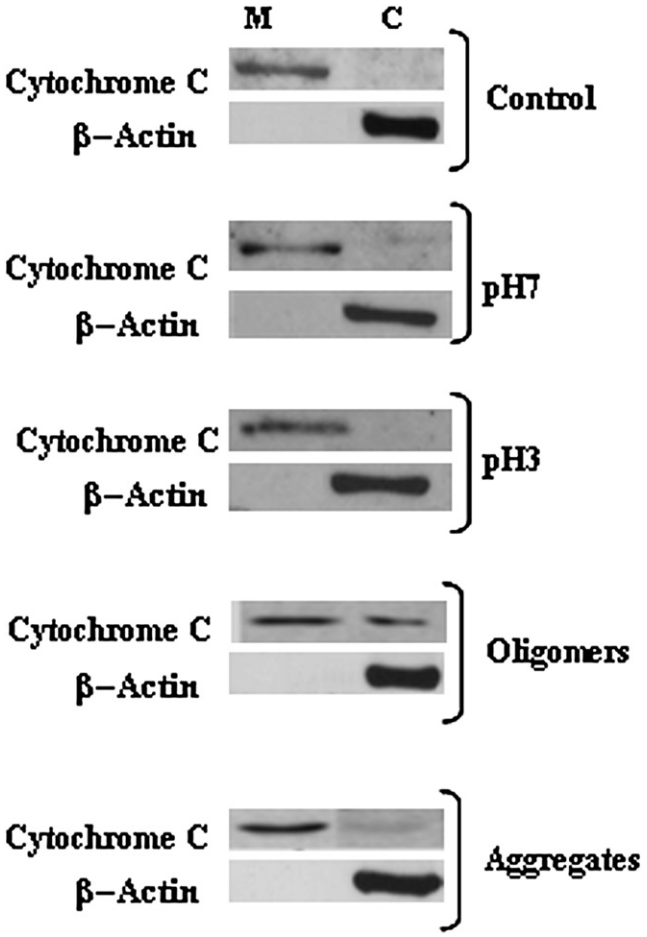

FIGURE 12 Cytochrome *c* is released in oligomer-treated LAN5 cells. Western blot of proteins extracted from mitochondrial (M) and cytosolic (C) fractions of LAN5 cells untreated or pH 3.1 or pH 7.2 buffer-treated cells or treated with oligomers or aggregates and incubated with anti-cytochrome *c* or anti-β-actin as control.

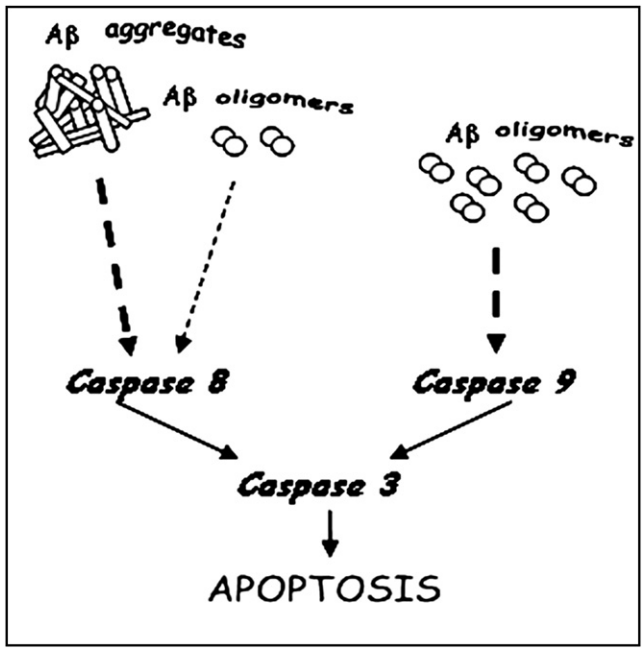

FIGURE 13 A sketched summary of the different actions by oligomers and fibrillar aggregates in LAN5 cell apoptosis activation. Aggregates, disturbing and/or obstructing the cellular membrane, activate the extrinsic apoptotic pathway upon caspase 8 and subsequently caspase 3 mediated signaling. Oligomers can induce apoptosis by caspase 8 activation, but principally promote cell stress, inducing the release of mitochondrial cytochrome *c* and activation of caspase 9 and subsequently caspase 3.

sites and seed the aggregation process similarly to what occurs during pathology. Moreover, it has been demonstrated that Aβ aggregates interact with their precursor and this leads to a toxic gain of function, possibly by inducing an APP conformational change that triggers cell death (25). Having detected localization of both rAβ42 and APP on the cell surface, we cannot exclude the possibility that rAβ42 was bound to its precursor to induce neurotoxicity in our in vitro experimental model. However, evidence indicates that monomeric and fibrillar forms of Aβ have the ability to bind to different membrane proteins, and some of these have been identified (26–28) Interactions between Aβ and one or more of these membrane proteins or receptors could directly or indirectly activate the apoptotic process, as demonstrated for receptor for advanced glycation end products, and may also contribute to fibrillogenesis (29,30). The ability to bind to different membrane proteins is in agreement with results obtained in previous studies in which D- and L-enantiomers of Aβ peptides were utilized. It was demonstrated that fibril toxicity was independent of the classical stereoisomeric specific ligand-receptor interaction, whereas fibril conformation, depending on its primary sequence, was a critical feature (31). A possible mechanism is that Aβ aggregates act as a membrane perturbant that alters the bilayer lipids and membrane-bound proteins or receptors, inducing activation of the cell death pathway (31).

Involvement of the mitochondrial path could be an explanation of the major toxicity of oligomers with respect to aggregates. Mitochondria are pivotal in controlling cell life and death (32). Perturbations in the physiological function of mitochondria inevitably disturb cell function and may initiate cell death. These are significant phenomena in the pathogenesis of a number of neurodegenerative disorders, including AD. Moreover, other evidence indicates that a mechanism of Aβ toxicity arises from its interaction with a mitochondrial target such as Aβ-binding alcohol dehydrogenase (33–35). However, it is known that the mitochondrial path is not the only source of intracellular toxicity. Indeed, intracellular Aβ is able to activate the intrinsic ER stress-induced apoptosis mediated by caspase 12 (36).

Furthermore, the possibility that different pathways are activated by the same sources is not an atypical condition; indeed, similar results were obtained by studies with air pollution particulate matter on lung epithelial cells (L132) (37). In that system, apoptosis activation was demonstrated both by TNF-a induced and by mitochondrial pathway.

However, different studies have implicated other known caspases in Aβ toxicity, and it has been demonstrated that activity by caspases 8 and 9 is required for APP cleavage and C-terminal peptide C31 generation, which are also involved in cell death (38,39).

In conclusion, the different amyloid species analyzed here cause neurotoxicity by distinct apoptotic mechanisms that take place in different parts of the cell. The evidence suggests that structural differences between Aβ oligomers and larger fibrillar aggregates may influence receptor-binding activity or the internalization mechanism, and promote activation of an extrinsic or intrinsic apoptotic pathway.

Finally, although activation of two different pathways is only a first step in establishing the major or minor toxicity of small oligomers with respect to larger species, the finding that pathology may be provoked by altered states of metabolic equilibrium may help in the development of new methods for early diagnosis, as well as new therapeutic strategies. In this context, progress in the emerging field of biomedical research called mitochondrial medicine, which involves the development of mitochondrial drugs and their delivery systems, could also lead to novel pharmacological treatments (40–42).

We thank Annalisa Pastore for relevant discussions and careful revision of the manuscript, and G. Spadaro, C. Sunseri, C. Dispensa, and S. Alessi for the assistance in the SEM experiments. The technical support of A. Pensato is also acknowledged.

This work is part of a research project, ''Neuropatie animali: analisi molecolari e funzionali della proteina prionica in razze bovine siciliane'' (project IZS SI 005/02), of the Italian Ministero della Salute.

REFERENCES

1. Mudher, A., and S. Lovestone. 2002. Alzheimer's disease—do Tauists and Baptists finally shake hands? *Trends Neurosci.* 25:22–26.
2. Lesne, S., M. T. Koh, L. Kotilinek, R. Kayed, C. G. Glabe, et al. 2006. A specific amyloid-β protein assembly in the brain impairs memory. *Nature*. 440:352–357.
3. Verdile, G., S. Fuller, C. S. Atwood, S. M. Laws, S. E. Gandy, et al. 2004. The role of β amyloid in Alzheimer's disease: still a cause of everything or the only one who got caught? *Pharmacol. Res.* 5:397–409.
4. Flament, S., A. Delacourte, and D. M. Mann. 1990. Phosphorylation of τ proteins: a major event during the process of neurofibrillary degeneration. A comparative study between Alzheimer's disease and Down's syndrome. *Brain Res.* 516:15–19.
5. Nunan, J., and D. H. Small. 2000. Regulation of APP cleavage by α-, β- and γ-secretases. *FEBS Lett*. 483:6–10.
6. Walsh, D. M., A. M. Minogue, C. Sala-Frigerio, J. V. Fadeeva, W. Wasco, et al. 2007. The APP family of proteins: similarities and differences. *Biochem. Soc. Trans.* 35:416–420.
7. Stoppini, M., A. Andreola, G. Foresti, and V. Bellotti. 2004. Neurodegenerative diseases caused by protein aggregation: a phenomenon at the borderline between molecular evolution and ageing. *Pharmacol. Res.* 50:419–431.
8. Georganopoulou, D. G., L. Chang, J. M. Nam, C. S. Thaxton, E. J. Mufson, et al. 2005. Nanoparticle-based detection in cerebral spinal fluid of a soluble pathogenic biomarker for Alzheimer's disease. *Proc. Natl. Acad. Sci. USA*. 15:2273–2276.
9. Selkoe, D. J. 1994. Alzheimer's disease: a central role for amyloid. *J. Neuropathol. Exp. Neurol.* 53:438–447.
10. Selkoe, D. J. 1994. Amyloid β-protein precursor: new clues to the genesis of Alzheimer's disease. *Curr. Opin. Neurobiol.* 4:708–716.
11. Walsh, D. M., and D. J. Selkoe. 2007. Aβ oligomers: a decade of discovery. *J. Neurochem.* 10:1471–1483.
12. Walsh, D. M., I. Klyubin, J. V. Fadeeva, W. K. Cullen, R. Anwyl, et al. 2002. Naturally secreted oligomers of amyloid β protein potently inhibit hippocampal long-term potentiation *in vivo*. *Nature*. 416:535–539.
13. Gong, Y., L. Chang, K. L. Viola, P. N. Lacor, M. P. Lambert, et al. 2003. Alzheimer's disease-affected brain: presence of oligomeric A β ligands (ADDLs) suggests a molecular basis for reversible memory loss. *Proc. Natl. Acad. Sci. USA*. 100:10417–10422.
14. Haass, C., and D. J. Selkoe. 2007. Soluble protein oligomers in neurodegeneration: lessons from the Alzheimer's amyloid β-peptide. *Nat. Rev. Mol. Cell Biol.* 8:101–112.
15. Carrotta, R., M. Manno, D. Bulone, V. Martorana, and P. L. San Biagio. 2005. Protofibril formation of amyloid β-protein at low pH via a noncooperative elongation mechanism. *J. Biol. Chem.* 280:30001–30008.
16. Carrotta, R., J. Barthès, A. Longo, V. Martorana, M. Manno, et al. 2007. Large size fibrillar bundles of the Alzheimer amyloid β-protein. *Eur. Biophys. J.* 36:701–709.
17. Carrotta, R., M. Di Carlo, M. Manno, G. Montana, P. Picone, et al. 2006. Toxicity of recombinant β-amyloid prefibrillar oligomers on the morphogenesis of the sea urchin *Paracentrotus lividus*. *FASEB J.* 20:1916–1927.
18. Berne, B. J., and R. Pecora. 1976. Dynamic Light Scattering with Application to Chemistry, Biology and Physics. Wiley, New York.
19. Schmitz, K. S. 1990. An Introduction to Dynamic Light Scattering by Macromolecules. Academic Press, New York.
20. Kerr, J. F., A. H. Wyllie, and A. R. Currie. 1972. Apoptosis: a basic biological phenomenon with wide-ranging implications in tissue kinetics. *Br. J. Cancer*. 26:239–257.
21. Lührs, T., C. Ritter, M. Adrian, D. Riek-Loher, B. Bohrmann, et al. 2005. 3D structure of Alzheimer's amyloid-β (1–42) fibrils. *Proc. Natl. Acad. Sci. USA*. 102:17342–17347.
22. Pillot, T., M. Goethals, M. Vanloo, C. Talussot, R. Brasseur, et al. 1996. Fusogenic properties of the C-terminal domain of the Alzheimer β-amyloid peptide. *J. Biol. Chem.* 271:28757–28765.
23. Crescenzi, O., S. Tomaselli, R. Guerrini, S. Salvatori, A. M. D'Ursi, et al. 2002. Solution structure of the Alzheimer amyloid β-peptide (1–42) in an apolar microenvironment. Similarity with a virus fusion domain. *Eur. J. Biochem.* 269:5642–5648.
24. Saavedra, L., A. Mohamed, V. Ma, S. Kar, and E. P. de Chaves. 2007. Internalization of β-amyloid peptide by primary neurons in the absence of apolipoprotein E. *J. Biol. Chem.* 282:35722–35732.
25. Lorenzo, A., M. Yuan, Z. Zhang, P. A. Paganetti, C. Sturchler-Pierrat, et al. 2000. Amyloid β interacts with the amyloid precursor protein: a potential toxic mechanism in Alzheimer's disease. *Nat. Neurosci.* 3:460–464.
26. Verdier, Y., M. Zarándi, and B. Penke. 2004. Amyloid β-peptide interactions with neuronal and glial cell plasma membrane: binding sites and implications for Alzheimer's disease. *J. Pept. Sci.* 10:229–248.
27. Boland, K., K. Manias, and D. H. Perlmutter. 1995. Specificity in recognition of amyloid-β peptide by the serpin-enzyme complex receptor in hepatoma cells and neuronal cells. *J. Biol. Chem.* 270:28022–28028.
28. Paresce, D. M., and R. N. Ghosh. 1996. Microglial cells internalize aggregates of the Alzheimer's disease amyloid β-protein via a scavenger receptor. *Neuron*. 17:553–565.
29. Yan, S. D., X. J. Chen Fu, M. Chen, H. Zhu, A. Roher, et al. 1996. RAGE and amyloid-β peptide neurotoxicity in Alzheimer's disease. *Nature*. 382:685–691.
30. Yan, S. D., A. Roher, M. Chaney, B. Zlokovic, A. M. Schmidt, et al. 2000. The biology of the receptor for advanced glycation end products and its ligands. *Biochim. Biophys. Acta*. 1502:145–157.

31. Cribbs, D. H., C. J. Pike, S. L. Weinstein, P. Velazquez, and C. W. Cotman. 1997. All-D-enantiomers of β-amyloid exhibit similar biological properties to all-L-β-amyloids. *J. Biol. Chem.* 272:7431–7436.

32. Chang, L. K., G. V. Putcha, M. Deshmukh, Jr., and E. M. Johnson. 2002. Mitochondrial involvement in the point of no return in neuronal apoptosis. *Biochimie*. 84:223–231.

33. Lustbader, J. W., M. Cirilli, C. Lin, H. W. Xu, K. Takuma, et al. 2004. ABAD directly links Aβ to mitochondrial toxicity in Alzheimer's disease. *Science*. 304:448–452.

34. Takuma, K., J. Yao, J. Huang, H. Xu, X. Chen, et al. 2005. ABAD enhances Aβ-induced cell stress via mitochondrial dysfunction. *FASEB J*. 19:597–598.

35. Yan, S. D., and D. M. Stern. 2005. Mitochondrial dysfunction and Alzheimer's disease: role of amyloid-β peptide alcohol dehydrogenase (ABAD). *Int. J. Exp. Pathol*. 86:161–171.

36. Nakagawa, T., H. Zhu, N. Morishima, E. Li, J. Xu, et al. 2000. Caspase-12 mediates endoplasmic-reticulum-specific apoptosis and cytotoxicity by amyloid-β. *Nature*. 403:98–103.

37. Dagher, Z., G. Garcon, S. Billet, P. F. Gosset, F. Ledoux, et al. 2006. Activation of different pathways of apoptosis by air pollution particulate matter (PM2.5) in human epithelial lung cells (L132) in culture. *Toxicology*. 225:12–24.

38. Lu, D. C., G. M. Shaked, E. Masliah, D. E. Bredesen, and E. H. Koo. 2003. Amyloid β protein toxicity mediated by the formation of amyloid-β protein precursor complexes. *Ann. Neurol*. 54:781–789.

39. Lu, D. C., S. Soriano, D. E. Bredesen, and E. H. Koo. 2003. Caspase cleavage of the amyloid precursor protein modulates amyloid β-protein toxicity. *J. Neurochem.* 87:733–741.

40. Larsson, N. G., and R. Luft. 1999. Revolution in mitochondrial medicine. *FEBS Lett*. 455:199–202.

41. Weissig, V., S. M. Cheng, and G. G. D'Souza. 2004. Mitochondrial pharmaceutics. *Mitochondrion*. 3:229–244.

42. Fischer, U., and K. Schulze-Osthoff. 2005. New approaches and therapeutics targeting apoptosis in disease. *Pharmacol. Rev*. 57:187–215.